Tunable large resonant absorption in a midinfrared graphene Salisbury screen

Min Seok Jang (장민석),[1,2,*] Victor W. Brar (韦小宝),[2,3,*] Michelle C. Sherrott,[2] Josue J. Lopez,[2] Laura Kim (김보영),[2] Seyoon Kim (김세윤),[2] Mansoo Choi (최만수),[1,4] and Harry A. Atwater[2,3,†]

[1]*Global Frontier Center for Multiscale Energy Systems, Seoul National University, Seoul 151-744, Republic of Korea*

[2]*Thomas J. Watson Laboratory of Applied Physics, California Institute of Technology, Pasadena, California 91125, USA*

[3]*Kavli Nanoscience Institute, California Institute of Technology, Pasadena, California 91125, USA*

[4]*Division of WCU Multiscale Mechanical Design, School of Mechanical and Aerospace Engineering, Seoul National University, Seoul 151-742, Republic of Korea*

(Received 24 March 2014; published 8 October 2014)

The optical absorption properties of periodically patterned graphene plasmonic resonators are studied experimentally as the graphene sheet is placed near a metallic reflector. By varying the size and carrier density of the graphene, the parameters for achieving a surface impedance closely matched to free-space ($Z_0 = 377\,\Omega$) are determined and shown to result in 24.5% total optical absorption in the graphene sheet. Theoretical analysis shows that complete absorption is achievable with higher doping or lower loss. This geometry, known as a Salisbury screen, provides an efficient means of light coupling to the highly confined graphene plasmonic modes for future optoelectronic applications.

DOI: 10.1103/PhysRevB.90.165409 PACS number(s): 78.67.Wj, 73.20.Mf, 78.20.Jq

The ability to interact strongly with light is important for a material to be useful in optics-based applications. Monolayer graphene exhibits a number of interesting optical phenomena, including a novel photothermoelectric effect [1,2], strong nonlinear behavior [3,4], and the potential for ultrafast photodetection [5]. However, the absolute magnitude of these effects is limited by the amount of light absorbed by the graphene sheet, which is typically 2.3% at infrared and optical frequencies [6,7]—a small value that reflects the single atom thickness of graphene. To increase the overall graphene-light interaction, many novel light scattering and absorption geometries have recently been developed. These include coupling graphene to resonant metal structures [8–13] or optical cavities where the electromagnetic fields are enhanced [14–16], or draping graphene over optical waveguides to effectively increase the overall optical path length along the graphene [17,18]. While those methods rely on enhancing interband absorption processes, graphene can also be patterned and doped so as to excite plasmonic modes that display strong resonant absorption in the terahertz to midinfrared regime [19–23]. Graphene plasmonic modes are highly sensitive to their environment, and they have been shown to display large absorption when embedded in liquid salts [19,24] or by sandwiching dopants between several graphene layers [23]. However, plasmonically active metallic and semiconductor structures can achieve near-perfect absorption of radiation at specified frequencies using a resonant interference absorption method [25–29]. The electromagnetic design of these structures derives in part from the original Salisbury screen design, but with the original resistive sheet replaced by an array of resonant metal structures used to achieve a low surface impedance at optical frequencies. It has recently been proposed that similar devices could be possible using graphene to achieve perfect absorption from terahertz to midinfrared [30,31]. Such a device would offer an efficient manner of coupling micron-scale free-space light into nanoscale plasmonic modes, and it would allow for electronic control of that coupling process. In this paper, we design and demonstrate a photonic heterostructure based on that principle, using tunable graphene nanoresonators placed a fixed distance away from a metallic reflector to drive a dramatic increase in optical absorption into the graphene.

A schematic of our device is shown in Fig. 1(a). A graphene sheet grown using chemical vapor deposition on copper foil is placed on a 1-μm-thick, low stress silicon nitride (SiN_x) membrane with 200 nm of Au deposited on the opposite side, which is used as both a reflector and a back-gate electrode. Nanoresonators with widths ranging from 20 to 60 nm are then patterned over $70 \times 70\,\mu m^2$ areas into the graphene using 100 keV electron beam lithography (see Sec. I in Supplemental Material) [32]. An atomic force microscopy (AFM) image of the resulting graphene nanoresonators is shown in the inset of Fig. 1(b). The device was placed under a Fourier transform infrared (FTIR) microscope operating in reflection mode, with the incoming light polarized perpendicular to the resonators in order to maximize the excitation of the resonant plasmon modes [20,22]. The carrier density of the graphene sheet was varied *in situ* by applying a voltage across the SiN_x between the gold and the graphene, and the resulting changes in resistance were continuously monitored using source and drain electrodes connected to the graphene sheet [Fig. 1(b)]. The carrier density of the graphene nanoresonators was determined from experimentally measured resonant peak frequencies (see Secs. II and III in the Supplemental Material [32]).

The total absorption in the device—which includes absorption in the SiN_x and the graphene resonators—is determined from the difference in the reflected light from the nanoresonator arrays and an adjacent gold mirror. For undoped and highly doped 40 nm nanoresonators, the total absorption is shown in Fig. 2(a), revealing large absorption at frequencies below $1200\,cm^{-1}$, as well as an absorption peak that varies strongly with doping at $1400\,cm^{-1}$ and a peak near $3500\,cm^{-1}$ that varies weakly with doping. In order to distill absorption features in the graphene from the environment (i.e., SiN_x and Au back reflector), we plot the difference in absorption

*These authors contributed equally to the work.

†haa@caltech.edu

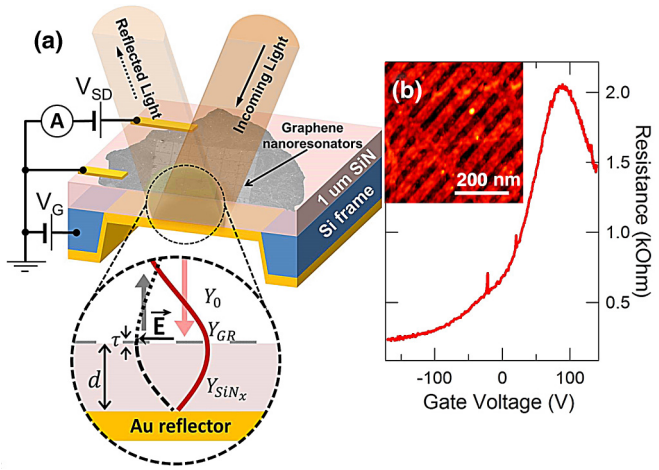

FIG. 1. (Color online) (a) Schematic device structure of graphene Salisbury screen. The inset illustrates the device with the optical waves at the resonance condition. (b) dc resistance of graphene as a function of the gate voltage. The inset is an AFM image of 40 nm nanoresonators.

between the undoped and doped nanoresonators, as shown in Fig. 2(b) for 40 nm nanoresonators. This normalization removes the low frequency feature below 1200 cm^{-1}, which is due to the broad optical phonon absorption in the SiN_x and is independent of graphene doping. The absorption feature at 1400 cm^{-1}, however, shows a dramatic dependence on the graphene sheet carrier density, with absorption into the graphene nanoresonators varying from near 0% to 24.5% as the carrier density is raised to 1.42×10^{13} cm^{-2}. Because the absorption increases with carrier density, we associate it with resonant absorption in the confined plasmons of the nanoresonators [19–22,33]. In Fig. 2(b), we also see that absorption at 3500 cm^{-1} exhibits an opposite trend relative to the lower energy peak, with graphene-related absorption decreasing with higher carrier density. This higher energy feature is due to interband graphene absorption, where electronic transitions are Pauli blocked by state filling at higher carrier densities [34]. For spectra taken from the bare, gate-tunable graphene surface, this effect leads to ~8% absorption, i.e., roughly twice the intensity observed from patterned areas. Finally, in Fig. 2(c), we investigated the graphene nanoresonator absorption as the resonator width is varied from 20 to 60 nm at fixed carrier density. This figure shows that the lower energy, plasmonic absorption peak has a strong frequency and intensity dependence on resonator width, with the maximum absorption occurring in the 40 nm ribbons.

The carrier density dependent plasmonic dispersion of this system is shown in Fig. 3(a). The observed resonance frequency varies from 1150 to 1800 cm^{-1}, monotonically increasing with larger carrier densities and smaller resonator widths. The plasmon energy asymptotically approaches ~1050 cm^{-1} due to a polar phonon in the SiN_x that strongly reduces the dielectric function of the substrate at that energy [35]. This coupling between the substrate polar phonon and the graphene plasmon has also been previously observed in back-gated SiO_2 devices [20,22,36]. In Fig. 3(b), we plot the intensity of the plasmonic absorption as a function of frequency at varying

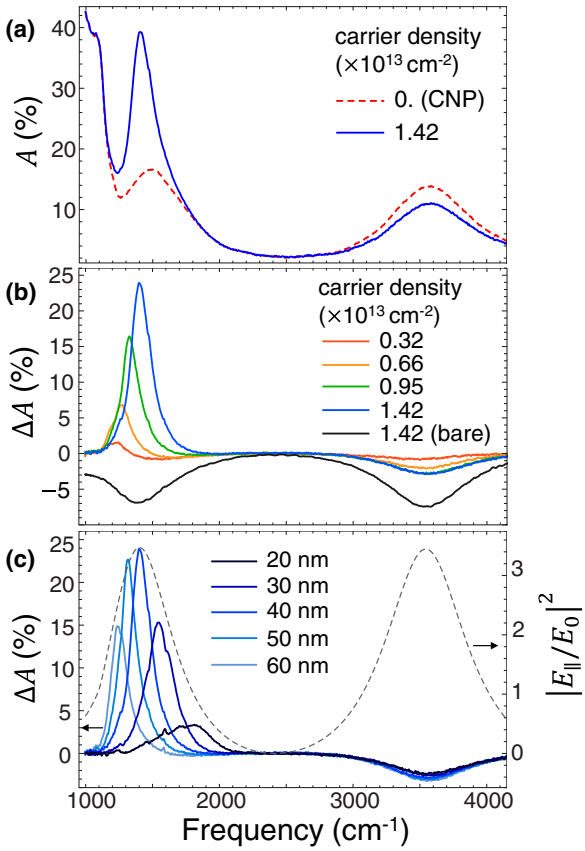

FIG. 2. (Color online) (a) The total absorption in the device for undoped (red dashed) and hole doped (blue solid) 40 nm nanoresonators. (b) The change in absorption with respect to the absorption at the charge neutral point (CNP) in 40-nm-wide graphene nanoresonators at various doping levels. The solid black curve represents the absorption difference of bare (unpatterned) graphene. (c) Width dependence of the absorption difference with the carrier concentration of 1.42×10^{13} cm^{-2}. The resonator width varies from 20 to 60 nm. The dashed curve shows the theoretical intensity of the surface parallel electric field at the SiN_x surface when graphene is absent.

carrier densities, revealing that for all carrier densities, the maximum in absorption always occurs at 1400 cm^{-1}.

The experimental behavior observed in Figs. 2 and 3 has some similarities with graphene plasmonic resonators patterned on back-gated SiO_2 devices; however, there are some significant differences. Most notably, the absolute absorption observed in this device is one order of magnitude greater than what has previously been observed. Furthermore, the maximum absorption in this device always occurs near 1400 cm^{-1}, in contrast to previous graphene plasmonic devices, where lower frequency resonances showed greater intensity due to fewer loss pathways and better k-vector matching between the graphene plasmons and free-space light [20,22]. These new absorption features can be understood by considering the role of the gold reflector. At 1400 cm^{-1}, the optical path length of the SiN_x is $\lambda/4n$, and the gold reflector creates a standing wave between the incident and reflected light that maximizes the electric field on the SiN_x surface. As a consequence, when the graphene nanoresonators are tuned to absorb at 1400 cm^{-1}, a double resonance condition is met, and the dissipation

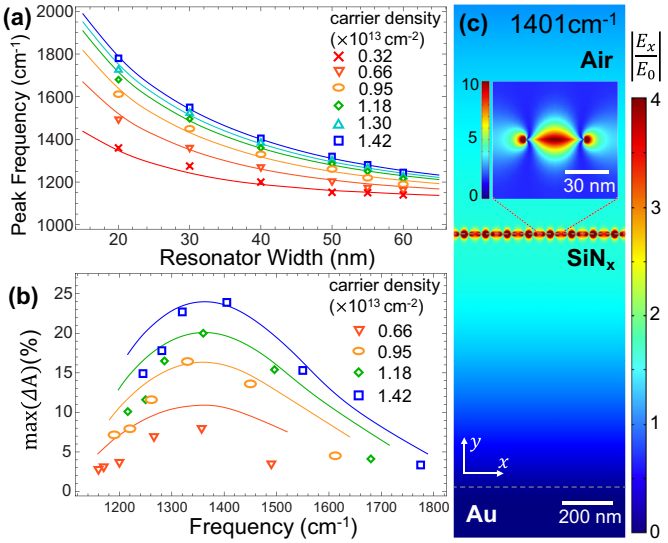

FIG. 3. (Color online) (a) Peak frequency as a function of resonator width. Solid curves and the symbols plot the theoretical and measured peak frequencies, respectively. (b) Frequency dependence of the experimental (symbols) and theoretical (curves) maximum absorption differences with varying doping level. (c) Theoretical electric field profile of a 40 nm graphene nanoresonator with the highest achieved carrier density ($1.42 \times 10^{13}\,\mathrm{cm}^{-2}$).

of the incoming radiation is greatly enhanced. Similarly, at $3500\,\mathrm{cm}^{-1}$, the second-order interference condition is met as the SiN_x optical path length becomes $3\lambda/4n$, maximizing the absorption due to interband transitions. In order to illustrate the role of the interference effect, the frequency dependence of the electric field intensity on the bare nitride surface is plotted as a dashed curve in Fig. 2(c). As can be seen in this figure, the intensity of the plasmonic absorption displays a frequency dependence that is similar to the calculated field intensity.

Full wave finite element electromagnetic simulations were performed in order to better understand the performance of our device and the underlying mechanisms driving the large observed absorption [20]. The conductivity of the graphene sheet was modeled using the local random phase approximation [37] with the intraband scattering rate Γ including both scattering by impurities Γ_{imp} and by optical phonons Γ_{oph}. By analyzing the absorption peak width when the resonance energy is much lower than the graphene optical phonon energy ($\sim 1600\,\mathrm{cm}^{-1}$), the impurity scattering rate is approximated to be $\Gamma_{\mathrm{imp}} = ev_F/\mu\sqrt{n\pi}$, with a carrier mobility of $550\,\mathrm{cm}^2/\mathrm{Vs}$ [33]. The rate of optical phonon scattering is estimated from the theoretically obtained self-energy $\Sigma_{\mathrm{oph}}(\omega)$, as $\Gamma_{\mathrm{oph}}(\omega) = 2\mathrm{Im}[\Sigma_{\mathrm{oph}}(\omega)]$ [22,33,38]. We note that the resulting theoretical plasmonic absorption curves have larger magnitude than the measured data. We attribute this discrepancy to experimental imperfections in the device, such as cracks in the graphene sheet that create electronically isolated resonators, tears in graphene or regions of contaminating residue where no resonators can be patterned, regions including grain boundaries or multilayer graphene that locally alter the graphene electronic structure [39], and missing resonators created during the lift-off process. Such effects are not included in our theoretical calculations, and in order to account for these imperfections, we introduce a fitting parameter of 0.72, which we multiply to the theoretical spectra. Our resulting theoretical curves for the frequency and intensity dependence of the resonant absorption are shown in Fig. 3(a) and 3(b), respectively. As seen in Fig. 3(b), the theory and the measurement show similar features—a maximum plasmonic absorption consistently occurs around $1400\,\mathrm{cm}^{-1}$ for a given charge density, regardless of the resonator width. The field profiles from our calculations are shown in Fig. 3(c), revealing a strong plasmonic response in the graphene nanoresonators for the $\lambda/4n$ condition, where the electric field is maximized on the surface, and the resonators match the correct resonance conditions.

A more complete understanding of the large resonant absorption observed in this graphene Salisbury screen comes from viewing the effect in terms of impedance matching, where the graphene metasurface is modified in such a way that it mimics a load whose admittance is close to the free-space wave admittance $Y_0 = \sqrt{\varepsilon_0/\mu_0}$, and thus allows for all incident light to be absorbed in the graphene sheet [40,41]. This description is diagrammed in the inset of Fig. 1(a). To understand this model, we can consider the effective admittance of a thin layer of thickness τ and admittance $Y_{\mathrm{GR}} = \sqrt{\varepsilon_{\mathrm{GR}}/\mu_{\mathrm{GR}}}$ sitting atop a dielectric with thickness d and admittance $Y_{\mathrm{SiN_x}}$ deposited on a reflecting mirror. For frequencies such that $d = m\lambda/4$ and for $\tau \ll 1$, the total effective admittance of the stack is given by $Y = -i\omega\varepsilon_{\mathrm{GR}}\tau$ (see Sec. V in Supplemental Material [32]). For normally incident light, the amount of absorption is given by $A = 1 - |(Y_0 - Y)/(Y_0 + Y)|^2$ when the layer is located a quarter wavelength away from the back reflector [41]. Thus, the absorption approaches unity as the relative admittance Y/Y_0 approaches 1.

Typically, the admittance of an unpatterned graphene sheet is quite low, and equivalent to its sheet conductivity σ. Thus, for unpatterned graphene, $Y = \sigma \approx e^2/4\hbar = \pi\alpha Y_0 \approx 0.023 Y_0$ when the photon energy is sufficiently higher than the Pauli-blocked interband transition energies, where α is the fine structure constant. As a result, the absorption by a pristine graphene monolayer in the Salisbury screen configuration can be calculated as $A \approx 8.8\% \approx 4\pi\alpha$, which is consistent with our experimental measurements of the bare graphene surface at $1400\,\mathrm{cm}^{-1}$ and $3500\,\mathrm{cm}^{-1}$ shown in Fig. 2(b).

With optical resonators patterned into the graphene layer, however, the surface admittance can be dramatically increased. When the resonators are sparsely spaced so that they barely interact with each other, one can obtain the effective permittivity of the resonator array by simply multiplying the spatial density of the resonators by the polarizability of an individual resonator $a(\omega)$. The admittance is then $Y = -i\omega a(\omega)/S$, where S is the area of the unit cell. Driven by the oscillating electric field of the incoming light, the charge carriers in graphene collectively move back and forth across the resonator. This charge oscillation leads to a Lorentzian line shape—centered at the plasmon resonance frequency—for the polarizability $a(\omega)$, as well as the surface admittance $Y(\omega)$. On resonance, strong charge oscillations maximize the dipole moment of the resonators, producing a dramatic increase in $\mathrm{Im}[a]$, while $\mathrm{Re}[a]$ crosses zero [31]. Recognizing that the absorption cross section of a dipole is $\sigma_{\mathrm{Abs}} = (\omega/c)\mathrm{Im}[a/\varepsilon_0]$, the surface admittance is given by $Y = (\sigma_{\mathrm{Abs}}/S)Y_0$ on resonance. This is physically intuitive because complete absorption occurs

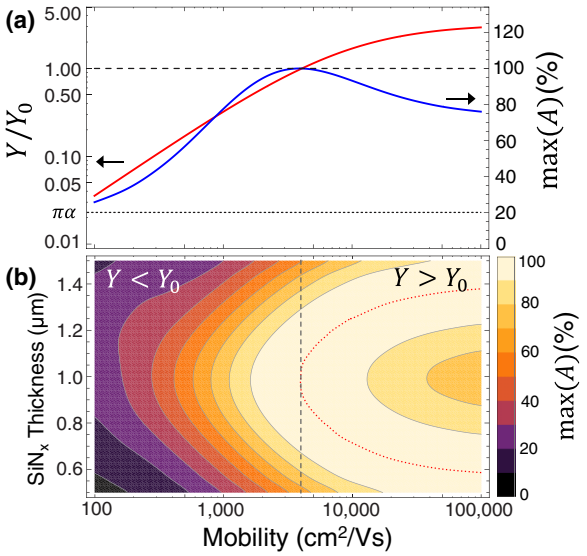

FIG. 4. (Color online) (a) Dependence of normalized surface admittance Y/Y_0 of 40 nm graphene nanoribbon array on resonance (red) and the maximum absorption (blue) on the carrier mobility μ (intraband scattering rate $\Gamma = ev_F/\mu\sqrt{n\pi}$). The SiN_x thickness and the pitch are assumed to be 1 μm and 80 nm, respectively. (b) Maximum absorption in the device as a function of the SiN_x thickness and the mobility. Impedance matching condition ($Y = Y_0$) is indicated as the gray dashed line. The red dotted curve indicates the condition for perfect absorption.

when the absorption cross section of the resonator array is large enough to cover the entire surface. As the resonators become closer to each other, the resonance frequency redshifts due to inter-resonator coupling, yet the condition for perfect absorption remains valid [31]. For our device at its highest doping level, σ_{Abs}/S is estimated to be $0.13Y_0$, which is much higher than $\pi\alpha$, and this allows for the large absorption we observe in our graphene nanoresonators shown in Fig. 2. Increasing carrier density leads to better coupling between the incoming light and the graphene plasmons, resulting in a stronger plasmon resonance. Therefore, at a given resonance frequency, higher doping enhances the absorption performance, as seen in Figs. 3(b) and S7.

Finally, we point out that the resonant absorption can be further increased if the resistive damping in the graphene is reduced. In Fig. 4(a), we plot the calculated carrier mobility dependence of the surface admittance for an array of graphene nanoribbons on a 1 μm SiN_x/Au layer. The highest achieved carrier density of $1.42 \times 10^{13}\,cm^{-2}$ is assumed, and the width of the ribbons is chosen to be 40 nm in order to match the plasmon resonance with the quarter wavelength condition of the SiN_x layer ($\sim 1400\,cm^{-1}$). Because the resonator absorption cross section increases as the graphene becomes less lossy, the resonant surface admittance increases with increasing mobility and crosses the free-space admittance Y_0 at a carrier mobility of $\mu \approx 4000\,cm^2/Vs$. As Y exceeds Y_0, the maximum absorption starts decreasing. However, it should be noted that in this high mobility regime, perfect absorption can still be achieved by shifting the quarter wavelength condition from the plasmon resonance frequency via changing the SiN_x thickness in order to decrease the coupling between the free wave and the graphene plasmon. To illustrate this, Fig. 4(b) shows the simulated peak absorption in the same resonator array as a function of both the mobility and the thickness of the nitride layer. Indeed, for $Y > Y_0$, the perfect absorption occurs at two different thickness values: one thinner and another thicker than 1 μm. This deviation becomes larger as the graphene mobility increases, and for mobilities reaching $10{,}000\,cm^2/Vs$, the device will show total absorption for nitride layers with thicknesses of 700 nm or 1.3 μm.

In summary, we have experimentally demonstrated that graphene plasmonic resonators placed a quarter wavelength away from a back reflector can absorb almost 25% of incoming midinfrared light, i.e., more than 10 times higher than the case of unpatterned graphene without a reflector (~2.3%) and 6–7 times higher than the extinction in graphene nanoresonators sitting on a conventional SiO_2/Si substrate [20,22]. The frequency and the amount of absorption can be largely tuned by controlling the plasmon resonance of the nanoresonators via electrostatic gating or varying the resonator size. This strong optical response allows for graphene to be an attractive platform for optoelectronic applications such as light modulators, detectors, and selective thermal emitters. Furthermore, our modeling predicts that modestly increasing the graphene mobility or decreasing the resonator line roughness can lead to 100% absorption, a tangible and important goal. These results demonstrate that the extremely small mode volumes of graphene plasmonic modes can be made accessible to free-space probes despite the large discrepancies in wavelength that suppress such coupling.

This work was supported by the Air Force Office of Scientific Research under Multidisciplinary University Research Initiative Awards No. FA9550-12-1-0488 (V.W.B.), FA9550-12-1-0024 (S.K. and L.K.K.), and the Department of Energy, Office of Science, under Grant No. DE-FG02-07ER46405 (M.C.S. and H.A.A.). M. S. Jang and M. Choi acknowledge support from the R&D Program of the Global Frontier Center for Multiscale Energy Systems funded by the National Research Foundation under the Ministry of Science, ITC & Future Planning, Korea (Grants No. 2011-0031561 and No. 2011-0031577). M. S. Jang acknowledges a postdoctoral fellowship from the POSCO T. J. Park Foundation. V. W. Brar gratefully acknowledges a postdoctoral fellowship from the Kavli Nanoscience Institute. M. C. Sherrott gratefully acknowledges graduate fellowship support from the Resnick Sustainability Institute at Caltech. S. Kim and M. S. Jang acknowledge support from a Samsung Fellowship.

[1] N. M. Gabor, J. C. W. Song, Q. Ma, N. L. Nair, T. Taychatanapat, K. Watanabe, T. Taniguchi, L. S. Levitov, and P. Jarillo-Herrero, Science **334**, 648 (2011).

[2] X. Xu, N. M. Gabor, J. S. Alden, A. M. van der Zande, and P. L. McEuen, Nano Lett. **10**, 562 (2009).

[3] H. Harutyunyan, R. Beams, and L. Novotny, Nat. Phys. **9**, 423 (2013).

[4] E. Hendry, P. J. Hale, J. Moger, A. K. Savchenko, and S. A. Mikhailov, Phys. Rev. Lett. **105**, 097401 (2010).

[5] F. Xia, T. Mueller, Y.-m. Lin, A. Valdes-Garcia, and P. Avouris, Nat. Nanotechnol. **4**, 839 (2009).

[6] R. R. Nair, P. Blake, A. N. Grigorenko, K. S. Novoselov, T. J. Booth, T. Stauber, N. M. R. Peres, and A. K. Geim, Science **320**, 1308 (2008).

[7] K. F. Mak, L. Ju, F. Wang, and T. F. Heinz, Solid State Commun. **152**, 1341 (2012).

[8] N. K. Emani, T.-F. Chung, A. V. Kildishev, V. M. Shalaev, Y. P. Chen, and A. Boltasseva, Nano Lett. **14**, 78 (2014).

[9] Y. Yao, M. A. Kats, P. Genevet, N. Yu, Y. Song, J. Kong, and F. Capasso, Nano Lett. **13**, 1257 (2013).

[10] Y. Yao, M. A. Kats, R. Shankar, Y. Song, J. Kong, M. Loncar, and F. Capasso, Nano Lett. **14**, 214 (2014).

[11] X. Zhu, L. Shi, M. S. Schmidt, A. Boisen, O. Hansen, J. Zi, S. Xiao, and N. A. Mortensen, Nano Lett. **13**, 4690 (2013).

[12] J. Kim, H. Son, D. J. Cho, B. S. Geng, W. Regan, S. F. Shi, K. Kim, A. Zettl, Y. R. Shen, and F. Wang, Nano Lett. **12**, 5598 (2012).

[13] M. Grande, T. Stomeo, G. V. Bianco, M. A. Vincenti, D. de Ceglia, V. Petruzzelli, G. Bruno, M. De Vittorio, M. Scalora, and A. D'Orazio, Appl. Phys. Lett. **102**, 231111 (2013).

[14] A. Majumdar, J. Kim, J. Vuckovic, and F. Wang, Nano Lett. **13**, 515 (2013).

[15] M. Furchi, A. Urich, A. Pospischil, G. Lilley, K. Unterrainer, H. Detz, P. Klang, A. M. Andrews, W. Schrenk, G. Strasser, and T. Mueller, Nano Lett. **12**, 2773 (2012).

[16] X. Gan, K. F. Mak, Y. Gao, Y. You, F. Hatami, J. Hone, T. F. Heinz, and D. Englund, Nano Lett. **12**, 5626 (2012).

[17] M. Liu, X. Yin, E. Ulin-Avila, B. Geng, T. Zentgraf, L. Ju, F. Wang, and X. Zhang, Nature **474**, 64 (2011).

[18] A. Pospischil, M. Humer, M. M. Furchi, D. Bachmann, R. Guider, T. Fromherz, and T. Mueller, Nat. Photon. **7**, 892 (2013).

[19] Z. Fang, S. Thongrattanasiri, A. Schlather, Z. Liu, L. Ma, Y. Wang, P. M. Ajayan, P. Nordlander, N. J. Halas, and F. J. García de Abajo, ACS Nano **7**, 2388 (2013).

[20] V. W. Brar, M. S. Jang, M. Sherrott, J. J. Lopez, and H. A. Atwater, Nano Lett. **13**, 2541 (2013).

[21] L. Ju, B. Geng, J. Horng, C. Girit, M. Martin, Z. Hao, H. A. Bechtel, X. Liang, A. Zettl, Y. R. Shen, and F. Wang, Nat. Nanotechnol. **6**, 630 (2011).

[22] H. Yan, T. Low, W. Zhu, Y. Wu, M. Freitag, X. Li, F. Guinea, P. Avouris, and F. Xia, Nat. Photon. **7**, 394 (2013).

[23] H. Yan, X. Li, B. Chandra, G. Tulevski, Y. Wu, M. Freitag, W. Zhu, P. Avouris, and F. Xia, Nat. Nanotechnol. **7**, 330 (2012).

[24] Z. Fang, Y. Wang, A. E. Schlather, Z. Liu, P. M. Ajayan, F. J. García de Abajo, P. Nordlander, X. Zhu, and N. J. Halas, Nano Lett. **14**, 299 (2014).

[25] J. A. Mason, S. Smith, and D. Wasserman, Appl. Phys. Lett. **98**, 241105 (2011).

[26] N. Liu, M. Mesch, T. Weiss, M. Hentschel, and H. Giessen, Nano Lett. **10**, 2342 (2010).

[27] Y. Avitzour, Y. A. Urzhumov, and G. Shvets, Phys. Rev. B **79**, 045131 (2009).

[28] C. Wu, B. Neuner, III, G. Shvets, J. John, A. Milder, B. Zollars, and S. Savoy, Phys. Rev. B **84**, 075102 (2011).

[29] N. I. Landy, S. Sajuyigbe, J. J. Mock, D. R. Smith, and W. J. Padilla, Phys. Rev. Lett. **100**, 207402 (2008).

[30] R. Alaee, M. Farhat, C. Rockstuhl, and F. Lederer, Opt. Express. **20**, 28017 (2012).

[31] S. Thongrattanasiri, F. H. L. Koppens, and F. J. García de Abajo, Phys. Rev. Lett. **108**, 047401 (2012).

[32] See Supplemental Material at http://link.aps.org/supplemental/10.1103/PhysRevB.90.165409 for more information on I. Device Fabrication, II. Electromagnetic Simulations, III. Determination of Carrier Density, IV. Peak Width Analysis, V. Derivation of Surface Admittance of a Thin Layer, and VI. Calculation of Surface Admittance of Graphene Nanoresonator Arrays.

[33] M. Jablan, H. Buljan, and M. Soljacic, Phys. Rev. B **80**, 245435 (2009).

[34] F. Wang, Y. B. Zhang, C. S. Tian, C. Girit, A. Zettl, M. Crommie, and Y. R. Shen, Science **320**, 206 (2008).

[35] G. Cataldo, J. A. Beall, H.-M. Cho, B. McAndrew, M. D. Niemack, and E. J. Wollack, Opt. Lett. **37**, 4200 (2012).

[36] E. H. Hwang, R. Sensarma, and S. Das Sarma, Phys. Rev. B **82**, 195406 (2010).

[37] L. A. Falkovsky and A. A. Varlamov, Eur. Phys. J. B **56**, 281 (2007).

[38] C.-H. Park, F. Giustino, M. L. Cohen, and S. G. Louie, Phys. Rev. Lett. **99**, 086804 (2007).

[39] Z. Fei, A. S. Rodin, W. Gannett, S. Dai, W. Regan, M. Wagner, M. K. Liu, A. S. McLeod, G. Dominguez, M. Thiemens, H. Castro NetoAntonio, F. Keilmann, A. Zettl, R. Hillenbrand, M. M. Fogler, and D. N. Basov, Nat. Nanotechnol. **8**, 821 (2013).

[40] G. T. Ruck, *Radar Cross Section Handbook* (Plenum Press, New York, 1970).

[41] R. L. Fante and M. T. McCormack, IEEE Trans. Antennas Propag. **36**, 1443 (1988).